Effect of End Groups and Grafting on the CO2Separation Performance of Poly(ethylene glycol) Based Membranes

ARTICLE *in* MACROMOLECULES · OCTOBER 2011

Impact Factor: 5.8 · DOI: 10.1021/ma201844y

3 AUTHORS, INCLUDING:

Tai-Shung Chung
National University of Singapore
727 PUBLICATIONS **19,578** CITATIONS

SEE PROFILE

Macromolecules

ARTICLE

pubs.acs.org/Macromolecules

Effect of End Groups and Grafting on the CO_2 Separation Performance of Poly(ethylene glycol) Based Membranes

Jianzhong Xia,[†,‡] Songlin Liu,[‡] and Tai-Shung Chung*[,‡]

[†]NUS Graduate School for Integrative Sciences and Engineering, National University of Singapore, 28 Medical Drive, Singapore 117456, Singapore

[‡]Department of Chemical and Biomolecular Engineering, National University of Singapore, 10 Kent Ridge Crescent, Singapore 119260, Singapore

ABSTRACT: Rubbery membranes have attracted significant attention for the CO_2/light gas separation due to their relative high permeability and high solubility selectivity. This work reports universal strategies to tailor CO_2 permeability and CO_2/light gas permselectivity via blending or grafting of poly(ethylene glycol) (PEG) derivatives into or onto organic−inorganic membrane (OIM) substrates. A PEG derivative is blended into the substrate which contains inorganic siloxane networks and poly(ethylene oxide) segments followed by thermal grafting. Ultrahigh CO_2 permeability (982 barrer at 45 °C) is achieved via physical blending, while extremely high CO_2 permeability (1840 barrer at 45 °C) is obtained after chemical grafting. Neither of these two modification methods shows the loss of CO_2/H_2 and CO_2/N_2 selectivity compared to the substrate. Melting and crystallization behaviors of this PEG derivative are believed to significantly affect the overall gas permeation performance. All the features make these OIMs promising membrane materials for CO_2 capture.

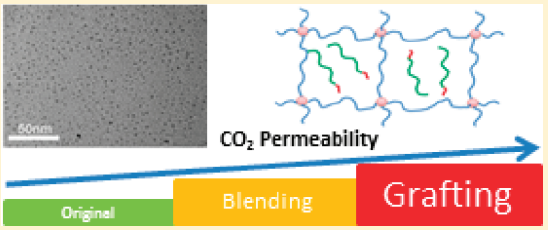

INTRODUCTION

Significant amounts of carbon dioxide (CO_2) have been generated from the combustion of coal and fossil fuels since the Industrial Revolution.[1] The increasing energy demand has further accelerated the process of CO_2 accumulation in the atmosphere. Recent extreme weather events have prompted the debate about effects of abnormal CO_2 concentration on the world's climate.[2] Reports show that almost 85% of the power consumed is generated by burning fossil fuel, which also emits a huge amount of CO_2.[3] In this scenario, technologies for the capture of CO_2 become essential to produce clean energy and furthermore to solve the dilemma between economy development and global warming.[4−6] Membrane technology has been proved to be a promising environmental friendly method for pre- and postcombustion CO_2 capture in the integrated gasification combined cycle (IGCC) coal-fired power stations.[7] According to specific technical assessments, CO_2/H_2 and CO_2/N_2 are the target separation gas pairs in precombustion and postcombustion, respectively.[6]

When membranes are employed as the separation tools, the flux (or permeability) and the separation factor (or selectivity) should be carefully evaluated. Ultrahigh CO_2 permeance is favorable instead of high CO_2/light gas selectivity according to the energy and cost analysis conducted by Merkel et al.[7] Conventional glassy membranes usually show relative lower CO_2 permeability with a CO_2/H_2 selectivity less than 1. In addition, glassy membranes will usually lose their CO_2/N_2 selective in mixed gas permeation due to CO_2 plasticization which facilitates the diffusivity of the slower gas.[8,9] Conversely, rubbery materials like silicon rubber[10,11] and poly(ethylene oxide) (PEO)[12−14] are more suitable for these separations because of the high CO_2/H_2 solubility selectivity and the relative inertness to CO_2 plasticization. PEO or poly(ethylene glycol) (PEG) based membranes possess a reversed selectivity of CO_2 to the much smaller H_2 molecules because of the polar and quadrupolar interactions between the ether oxygen (EO) unit and the CO_2 molecules.[13] One strategy to enhance the CO_2/light gas selectivity is to introduce more EO groups into the polymer matrix. However, increasing highly polar EO moieties result in crystallinity, thus leading to a decrease in free volume and lower permeability.[12] In addition, CO_2/H_2 selectivity might be compromised by the increase in size sieving ability. On the other hand, size sieving is favorable for the CO_2/N_2 selectivity because the size of CO_2 is smaller than that of N_2. Overall, designing a membrane with a higher permeability is still the major challenge.

Many methods have been reported to increase or maintain the gas permeability upon increasing EO group concentration. Crystallization of EO segments could be prevented in the copolymer if the length of the EO chain is short.[15] By cross-linking poly(ethylene glycol diacrylate) (PEGDA), Lin et al.[16] have synthesized a series of amorphous copolymer networks and achieved CO_2 permeability over 400 barrer with CO_2/H_2 selectivity of 31 at −20 °C. In order to obtain PEO based membranes with higher permeability, an easier way is to simply incorporate PEG into the polymeric matrix which already has reasonable CO_2/H_2 and CO_2/N_2 selectivity.[17−23] Kawakami et al.[17] directly embedded a low molecular weight PEG (M_w = 300 g/mol) into

Received: August 11, 2011
Revised: August 25, 2011
Published: September 07, 2011

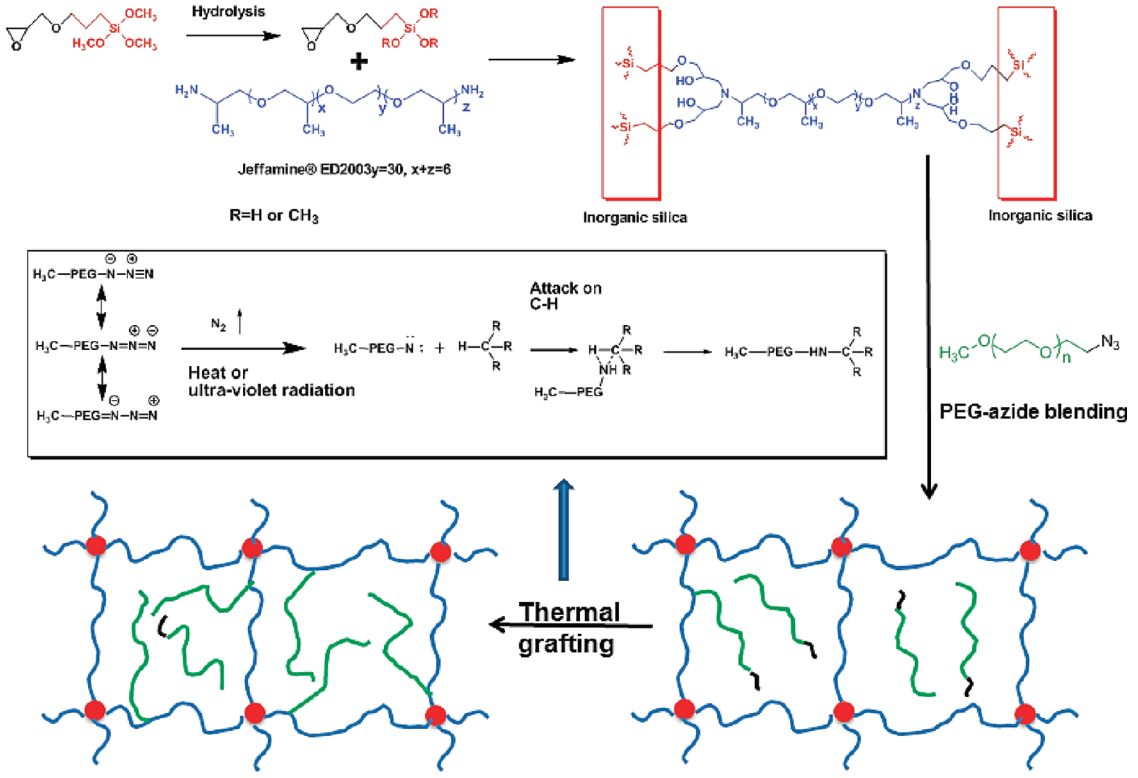

Figure 1. Synthetic route of OIMs containing PEG-azide and the subsequent thermal reactions.

the microporous region of cellulose membranes and obtain a CO_2 permeability of 82 barrer. Car et al.[18−20] and Yave et al.[21−23] have blended low molecular weight PEG into thermoplastic poly(amide-*b*-ethylene oxide) (PEBAX) and poly(ethylene oxide)−poly(butylene terephthalate) (PEO−PBT) multiblock copolymers and obtain promising results.

In order to achieve optimized overall performance, the matrix should have the following characteristics: (1) be homogeneous with blended PEG; (2) lower permeation resistance; (3) sufficient mechanical strength after blending; (4) already has CO_2/light gas selectivity. The aforementioned works involving PEBAX and PEO−PBT have met some of requirements; however, a new family of organic−inorganic membranes (OIMs) with CO_2 permeability of 300−492 barrer and CO_2/H_2 selectivity of 8−9 developed by Shao and Chung[24] may become a superior candidate for the same strategy. Our previous works had successfully enhanced the separation performance of this matrix by using both physical blending[25] and solution-state chemical grafting.[26] These OIMs with PEG up to 60 wt % demonstrated CO_2 permeability of 845 barrer with CO_2/H_2 and CO_2/N_2 permselectivity around 10 and 40, respectively. However, their performance could still be further improved by eliminating hydrogen bonding using non-hydroxyl groups as the end groups according to the trend reported by Yave et al.[21] By modifying OIMs with O-zone-initiated polymerization of poly(ethylene glycol methacrylate) (PEGMA), Lau et al.[26] have achieved CO_2 permeability of 1920 barrer in mixed gas permeation tests. Thus, in this study two kinds of methoxy-PEG-azide (M_w = 350 and 1100) have been employed to replace PEG for comparison of end groups. Furthermore, azide functional groups provide us the freedom to investigate the effect of PEG grafting on the overall gas permeation performance because they are reactive to the C−H bond.

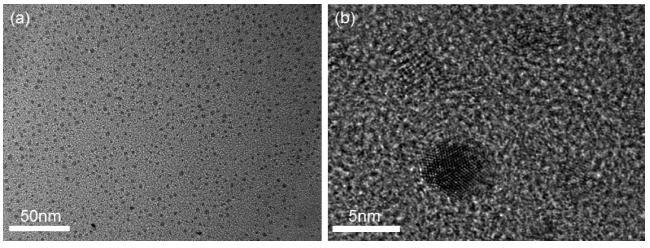

Figure 2. TEM micrography of GP w/o PEG-azide at (a) a low magnitude and (b) a high magnitude.

Because of the high crystallization tendency of higher molecular weight PEG, OIMs with PEG-azide1100 are not amorphous at ambient temperature. Therefore, the investigation on temperature dependence of gas permeation has also been carried out.

EXPERIMENTAL SECTION

1. Materials. JeffamineED-2003 (*O*,*O*′-bis(2-aminopropyl)poly(propylene glycol)-*block*-poly(ethylene glycol)-*block*-poly(propylene glycol), M_w: 2000 g/mol), ethanol (AR grade), and 3-glycidyloxypropyltrimethoxysilane (GOTMS) were purchased from Sigma-Aldrich and used as received. Methoxy-PEG-azide (M_w: 350 and 1100 g/mol) were ordered from Creative PEGWorks and used without further treatment. Concentrated hydrochloric acid from Fisher Scientific was employed as the catalyst for the hydrolysis of GOTMS. High-purity compressed H_2 (99.999%), N_2 (99.999%), CO_2 (99.98%), and CO_2/N_2 (50:50) mixed gases were purchased from SOXAL, Singapore.

2. Membrane Preparation. The syntheses of OIMs involve hydrolysis of GOTMS followed by polycondensation reactions. Figure 1 shows the synthetic route of OIMs containing PEG-azide and the

Table 1. Thermal Properties of GPA1100 Series

samples	T_g (°C)	T_{m2p} (°C)[a]	T_{c2p} (°C)[b]	$-\Delta H_c$ (J/g)[c]	$-\Delta H'_c$ (J/g)[d]
GP w/o PEG-azide	NA	24.5	−24.5	51	
GPA1100-20	−51.9	41.1	2.5	76	71
GPA1100-40	−54.2	42.1	16.1	95	91
PEG-azide1100	NA	45.1	22.5	153	

[a] Peak melting temperature of the second heating curve. [b] Peak crystallization temperature of the second cooling curve. [c] ΔH_c is the heat of crystallization obtained experimentally from DSC. [d] $\Delta H'_c$ is the theoretical value calculated by eq 3.

Table 2. Pure Gas Permeability and Selectivity of OIMs Blended with PEG-azide

sample	temp (°C)	H_2 permeability (barrer)[a]	N_2 permeability (barrer)	CO_2 permeability (barrer)	CO_2/H_2 selectivity	CO_2/N_2 selectivity
GP w/o PEG-azide	35	33	6.3	275	8.2	44
	45	49	9.9	344	7.0	35
GPA350-20	35	54.5 (36)[b]	12.6 (7.3)	530 (333)	9.5 (9.3)	41 (46)
	45	77.5 (53)	19.3 (11.7)	634 (413)	8.2 (7.8)	33 (35)
GPA350-40	35	70.7 (37)	20.4 (7.5)	750 (363)	10.6 (9.7)	37 (48)
	45	101 (54)	29.8 (11.9)	913 (455)	9.0 (8.5)	31 (38)
GPA1100-20	45	62 (61)	13.9 (13.4)	468 (474)	7.5 (7.8)	34 (35)
GPA1100-40	45	91 (80)	22.6 (18.3)	982 (662)	10.8 (8.3)	43 (36)

[a] 1 barrer = 10^{-10} cm^3 (STP) cm/(cm^2 s cmHg). [b] Data in the parentheses are from ref 25 where PEG 400 and 1000 were used. In other words, GPA350 and GPA1100 series are compared with GPP400 and GPP1000 series, respectively.

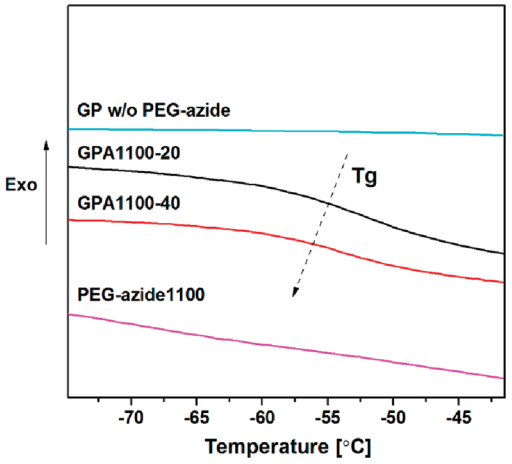

Figure 3. Glass transition temperature shifts of GPA1100 series by DSC.

subsequent thermally induced reactions. In order to fully hydrolyze GOTMS, the molar ratio of GOTMS, ethanol, water, and hydrochloric acid has to be kept as 1:1.13:3.2:0.05. After being stirred at ambient temperaure for 60 min, the hydrolyzed solution was then transferred to a water/ethanol (30/70 wt %) mixed solvent which contains 2 wt % of Jeffamine ED-2003. The exact usage of each component has been carefully calculated in order to maintain the molar ratio of GOTMS to Jeffamine ED-2003 at 4:1. Afterward, the solution was fluxed at 60 °C for 1 h. PEG-azide was added into the mixture and stirred for 10 min before the solution was poured into a Teflon dish. After solvent evaporation at 30 °C for 1 day and 40 °C for 2 days, these OIMs were dried in a vacuum oven at 70 °C overnight in order to complete the condensation reactions. The Teflon dish was then sealed in a plastic zig bag and put in a refrigerator (−20 °C) for 6 h. Finally, these OIMs blended with PEG-azide were peeled off and stored in a desiccator before any characterizations. Thermal grafting was performed in a vacuum furnace by temperature ramping from ambient temperature to 140 °C by 1 °C/min

Table 3. Solubility and Diffusivity Coefficients of GPA1100 and GPP1000 Series at 45 °C

	S_{CO_2} (cm^3 STP/(cm^3 atm))		D_{CO_2} (cm^2/s) × 10^6	
PEG blended (%)	GPP1000	GPA1100	GPP1000	GPA1100
0	1.16	1.16	2.26	2.26
20	1.17	1.17	3.07	3.05
40	1.27	1.29	3.97	5.79

and holding for 12 h. The thickness of obtained membranes ranges from 150 to 300 μm.

3. Measurements of Gas Permeation Properties. A constant volume method was employed to obtain the pure gas permeability,[27] and the solution-diffusion mechanism was used to explain the gas transport properties through dense membranes.[8] Thus, the permeability (P) can be expressed as

$$P = D \times S \tag{1}$$

where D and S are the diffusivity and solubility coefficients, respectively. The ideal selectivity of membranes for pure gases A and B is defined as follows:

$$\alpha_{A,B} = \frac{P_A}{P_B} = \left[\frac{D_A}{D_B}\right] \times \left[\frac{S_A}{S_B}\right] \tag{2}$$

H_2, N_2, and CO_2 permeability was measured. The temperature was gradually increased from 30 to 50 °C, and the testing pressure for all the membranes was 2 atm. The rate of pressure increase (dp/dt) at steady state was used for the calculation of gas permeability according to the equation

$$P = \frac{273.15 \times 10^{10}}{760} \frac{Vl}{AT(p \times 76/14.7)}\left(\frac{dp}{dt}\right) \tag{3}$$

where P is the gas permeability in barrer (1 barrer = 1 × 10^{-10} cm^3 (STP) cm/(cm^2 s cmHg)), V is the volume of downstream chamber

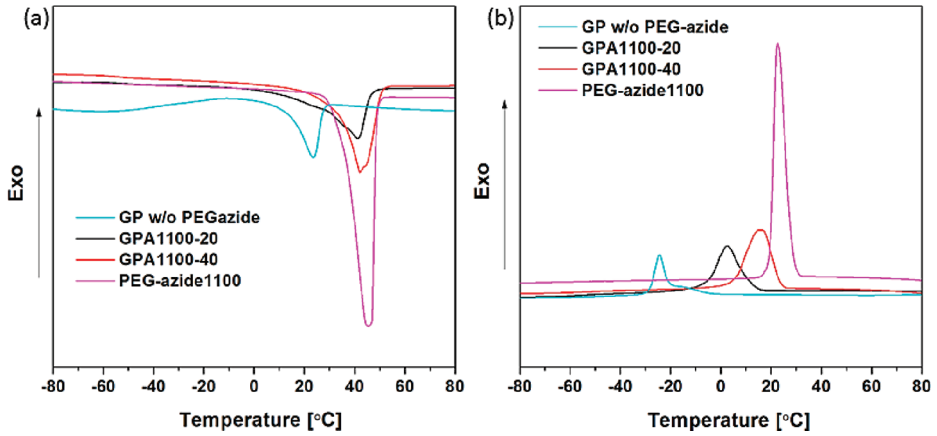

Figure 4. DSC curves of (a) second heating and (b) second cooling of GPA1100 series.

(cm^3), l is the membrane thickness (cm), A is the effective area of membrane (cm^2), T is the operating temperature (K), and p is the upstream operating pressure (psia). The mixed gas permeation properties for these hybrid membranes were obtained with a homemade mixed gas permeation cell as described in the work of Xia et al.[25] Samples were tested with a CO_2/N_2 (50%/50% mole fraction) binary gas and analyzed by gas chromatography at 45 °C with a total pressure of 4 atm. The gas permeability of CO_2 and N_2 is calculated by following equations:

$$P_{CO_2} = \frac{273.15 \times 10^{10}}{760} \frac{y_{CO_2} Vl}{AT(76/14.7)(x_{CO_2} p)} \left(\frac{dp}{dt}\right) \quad (4)$$

$$P_{N_2} = \frac{273.15 \times 10^{10}}{760} \frac{(1 - y_{CO_2})Vl}{AT(76/14.7)[(1 - x_{CO_2})p]} \left(\frac{dp}{dt}\right) \quad (5)$$

where y_{CO_2} is the mole fraction of CO_2 in the feed gas and x_{CO_2} is the mole fraction of CO_2 in the permeate.

4. Measurements of Gas Sorption. Sorption measurements from 30 to 50 °C were conducted by using the gravimetric sorption technique (Cahn D200 microbalance sorption cell) which could be found elsewhere.[28] The sorption cell loaded with ~70 mg samples was evacuated overnight prior to sorption testing. From the weight gain, the amount of gas absorbed could be obtained after buoyancy correction. Therefore, the solubility coefficient could be obtained by fitting the slope of the sorption isotherms. The diffusivity of gas penetrants was then calculated from solubility and permeability according to eq 1.

5. Characterizations. DSC was performed on a DSC822 (Mettler Toledo) from −100 to 100 °C with a heating and cooling rate of 10 °C/min. Two heat cycles of each membrane were performed, and the glass transition temperature was obtained from the second heating cycle. Ultrathin films obtained from diluted solutions (0.01 wt %) are used for the transmission electron microscope (TEM) characterization. The procedure is the same as the thick membrane preparation. A wide-angle X-ray diffractometer (Bruker D8 series) was employed to determine the crystallinity at ambient temperature. Ni-filtered Cu Kα radiation with a wavelength of 1.54 Å was used. The d-spacing was calculated based on the Bragg's law $n\lambda = 2d \sin\theta$, where n is the integral number, λ is the wavelength, d is the dimension spacing, and 2θ is the diffraction angle. The chemical structure changes of OIMs with PEG-azide after thermal grafting were characterized by solid-state ^{13}C NMR (100.6 MHz) with magic angle spinning (MAS) at 7.5 kHz performed on a Bruker DRX 400 spectrometer. The nitrogen 1s bonding energy change after thermal grafting was monitored by an XPS spectrometer (Kratos Analytical Ltd., England) under ultrahigh vacuum. All spectra were obtained at a photoelectron takeoff angle vertical to the sample.

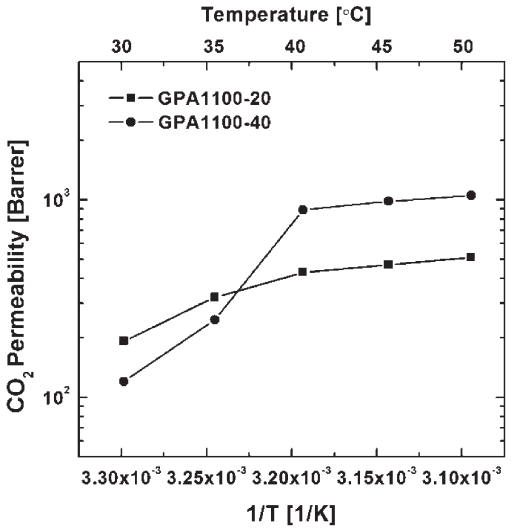

Figure 5. Temperature dependence of CO_2 permeability of GPA1100 series.

RESULTS AND DISCUSSION

1. Basic Physicochemical Properties. These reverse-selective OIMs are constructed by employing the in situ formed siloxane inorganic networks as the cross-linking junctions. The organic segments containing PEO chains are immobilized by these inorganic contents as shown in Figure 1. The inorganic components (black spots) are dispersed homogenously in the organic phase as indicated by the TEM micrograph in Figure 2a. The lattice features inside of the black spot as shown in Figure 2b prove that the inorganic siloxane networks have been successfully synthesized. The micromorphology analysis in detail regarding the shape and the size distribution could be found in our previous work.[25] PEG-azides of M_w 350 and M_w 1000 were blended into the pristine substrate (also referred as GP w/o PEG-azide). The blended hybrid OIMs are labeled by GPAX-Y, in which GPA represents the GOTMS-PEO PEG-azide blend, X represents the molecular weight of blended PEG, and Y represents the weight percentage of the blended PEG. For example, GPA1100-20 means the OIM contains 20 wt % of PEG-azide 1100 g/mol.

It is well-known that PEGs and their derivatives have a strong crystallization tendency due to the highly polar ethylene oxide

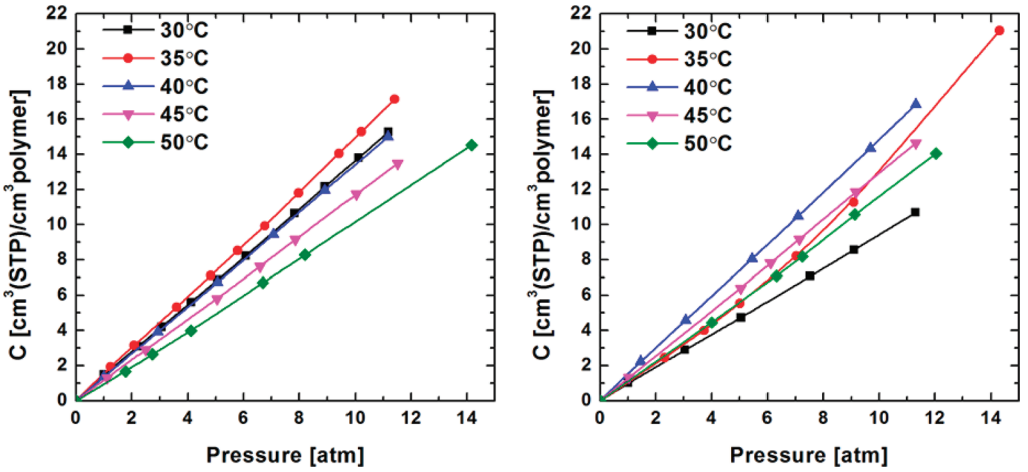

Figure 6. Temperature dependences of CO_2 sorption isotherms of (a) GPA1100-20 and (b) GPA1100-40.

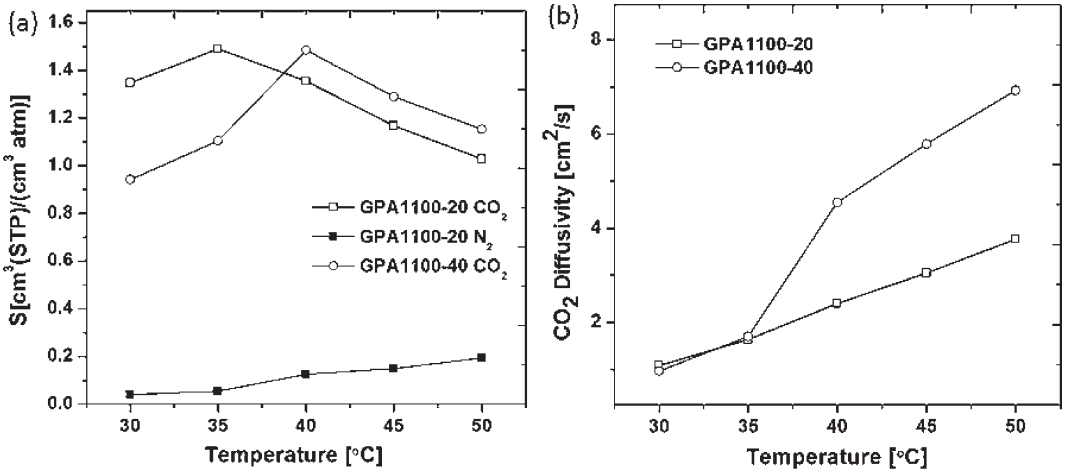

Figure 7. Temperature dependence of (a) solubility and (b) CO_2 diffusivity of GPA1100-20 and GPA1100-40.

moieties. Meanwhile, the melting temperatures and crystallization temperatures of these PEG based materials are close to the ambient temperature, which makes the thermal history of these OIMs very unclear. Therefore, all the OIMs employed in this study were cooled to −20 °C first and then naturally warmed up to ambient temperature prior to all characterizations. Because of the cooling induced crystals, GPA1100 series are translucent even at ambient temperature due to the relative high melting temperature of PEG-azide1100 (above 25 °C), as shown in Table 1. The membranes of GP w/o PEG-azide and GPA350 series are transparent due to their lower melting temperatures (below 25 °C).

2. Gas Transport Properties of OIMs with Physical Blending. Previous studies show that both CO_2 permeability and CO_2/H_2 selectivity could be enhanced by adding a low molecular weight PEG into an existing CO_2 selective material.[17−23,25] However, this kind of enhancement reaches a limit when hydroxyl-terminated PEG (normal PEG) is employed. High cohesive energy caused by the hydrogen bonding between the hydroxyl groups and the EO groups inhibits further improvement on the CO_2 diffusivity. In this work, PEGs terminated with methoxy group and azide group are used to replace the normal PEG. According to the previous work,[25] the molecular weight of the blended PEG has significant effect on gas permeation performance. Therefore, only PEG-azides with similar molecular weights are used. GPA350 and GPA1100 series (here A represents PEG-azide) are compared with GPP400 and GPP1000 series in our previous work (the last P represents PEG), respectively. For easy comparison, only the permeability data when the membranes are in amorphous status are listed (Table 2).

With the addition of PEG-azide, the permeability of CO_2 as well as other gases shows surprising increments of up to 100%, compared to those blended with normal PEG. The permeability improvement increases with more loading. Sorption studies show that solubility is enhanced with more PEG-azide loading. Diffusivity calculated based on the solution-diffusion mechanism shows improvement as well. The solubility enhancement could be attributed to a higher EO group density, while the diffusivity increment could be ascribed to the increasing chain flexibility as indicated by the decreasing glass transition temperature as shown in Figure 3.

The permeability increment of samples with lower molecular weights (GPP400 to GPA350 series) is greater than that of the higher molecular weight samples (GPP1000 to GPA1100 series) after replacing hydroxyl groups with azide groups. This is due to the fact that the end group concentrations are higher in GPA350

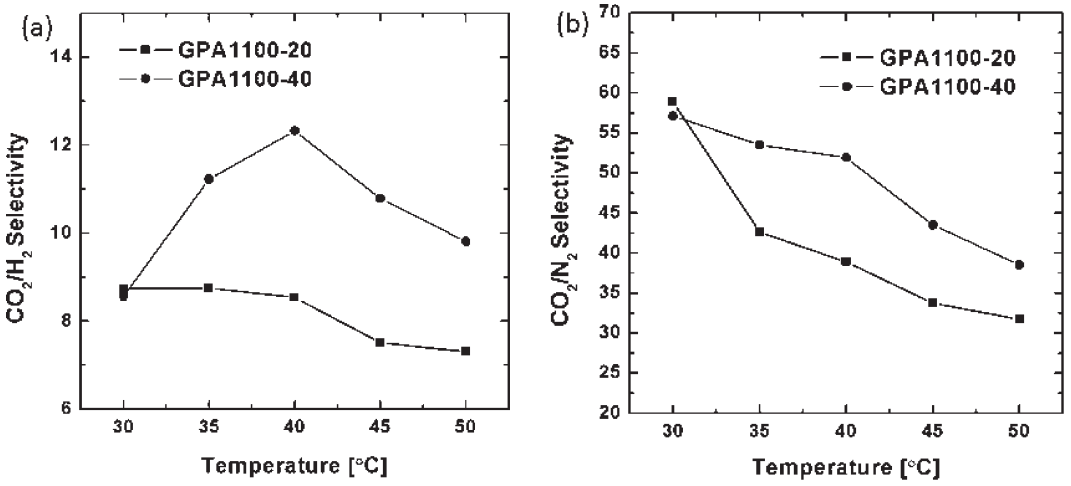

Figure 8. Temperature dependence of (a) CO_2/H_2 and (b) CO_2/N_2 selectivity of GPA1100-20 and GPA1100-40.

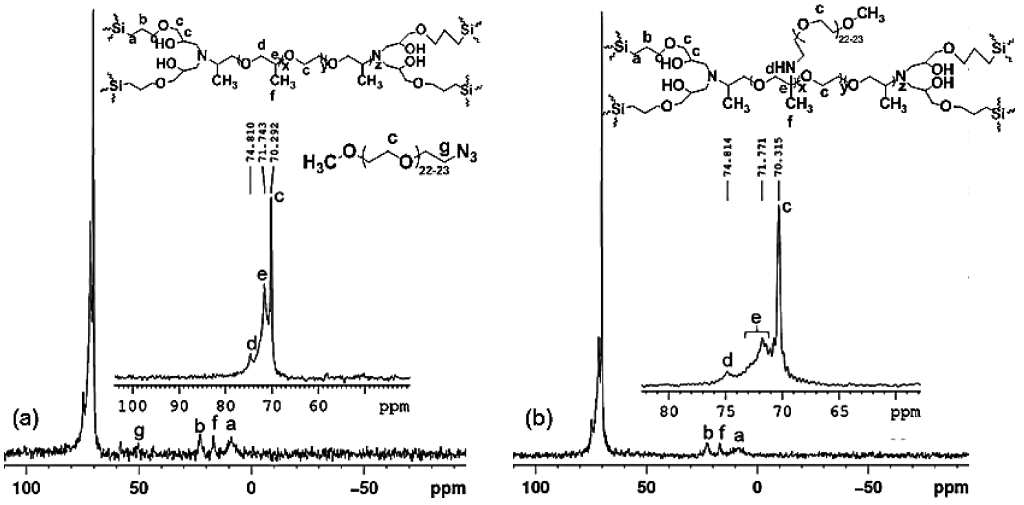

Figure 9. ^{13}C solid-state NMR spectra of (a) GPA1100-40 pristine and (b) GPA1100-40 after thermal grafting.

and GPP400 than those in GPA1100 and GPP1000 at the same loading. Without hydrogen bonding, the chain flexibility increases; thus, the diffusivity of CO_2 in GPA350 and GPA1100 increases as shown in Table 3. The CO_2 solubility of GPA1100 series also increases slightly compared to that of GPP1000 series because more EO moieties are able to interact with CO_2 after eliminating hydrogen bonding. The CO_2/H_2 permselectivity increases because of the increased solubility selectivity. On the other hand, the size sieving effect has also been weakened because the polymer chains are more flexible after eliminating hydrogen bonding. The slight decrease of CO_2/N_2 selectivity except GPA1100-40 are ascribed to the weakened size sieving effect because the kinetic diameter of CO_2 (3.3 Å) is smaller than that of N_2 (3.64 Å). The solubility and diffusivity of OIMs blended with 20 wt % PEG and PEG-azide are almost the same because the effect of replacing end group is not so obvious due to their low PEG loadings.

GPA1100-40 is also evaluated by a binary gas mixture of CO_2/N_2 (50:50 mole fraction) at 45 °C. Similar to our previous work,[25] CO_2 permeability (998 barrer) is comparable to that of the pure gas (982 barrer), while N_2 permeability increases from 22.6 to 31.5 barrer. Therefore, CO_2/N_2 selectivity decreases from 43 to 32, which is caused by the CO_2 plasticization.[29]

3. Thermal Properties of GPA1100 Series. Thermal properties of polymeric membranes are critical to the gas permeation performance. This is specially ture for the PEO-based rubbery membranes because they are highly crystallizable materials, and their melting temperatures are close to the normal permeation testing temperatures, 35 °C. Because of their structure similarity, PEG-azide and PEO segments of GP w/o PEG-azide could crystallize with each other as revealed by the heat of crystallization analysis. In Table 1, ΔH_c is the heat of crystallization experimentally obtained from DSC, while $\Delta H'_c$ is the theoretical value calculated using eq 6 by assuming cocrystallization.

$$\Delta H'_c = \Delta H_c(a) \times \text{wt }\%(\text{PEG-azide}) + \Delta H_c(b) \times (1 - \text{wt }\%(\text{PEG-azide})) \quad (6)$$

where $\Delta H_c(a)$ is the heat of crystallization of pure PEG-azide and $\Delta H_c(b)$ is the heat of crystallization of GP w/o PEG-azide. The experimental value is comparable to the theoretical value. Figure 4a,b shows the second heating and second cooling DSC curves of GPA1100 series. GP w/o PEG-azide and pure PEG-azide1100 are also included for comparison. A melting point depression (MPD) is observed for GPA1100 series as shown in

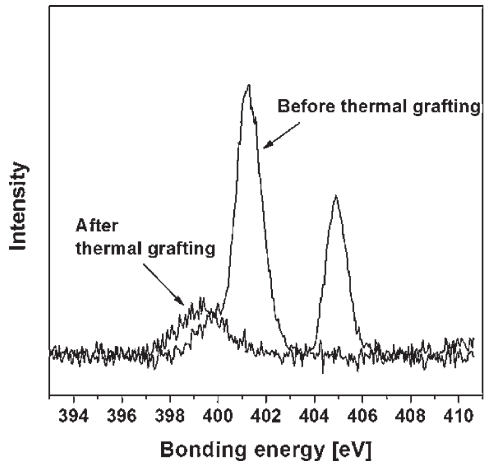

Figure 10. N 1s XPS data before and after thermal grafting for GPA1100-40.

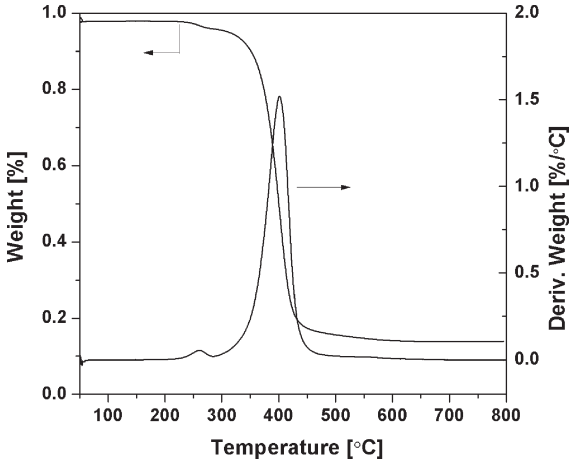

Figure 11. TGA data of GPA1100-40 before thermal grafting.

Table 1. Similar to the crystallization behavior of crystallizable block copolymers, the MPD in our case could be caused by the confined crystallization of PEG-azide in the OIMs.[30] The extending of the PEG-azide crystals is restricted by the cross-linked network, which would result in the melting temperature decrease. The crystallization peaks of GPA1100 series located between the peaks of GP w/o PEG-azide and pure PEG-azide. That the lowest crystallization temperature belongsto GP w/o PEG-azide indicates its lowest crystallization tendency because the PEO segments in the GP w/o PEG-azide are immobilized by cross-linking. When PEG-azide1100, which has the similar molecular weight to the PEO segments in the matrix, is added into the matrix, cocrystallization happens. PEG-azide1000 plays the role like crystallization intermediate between two PEO segments so that the membrane becomes easy to crystallize. When more PEG-azide is added, the crystallization tendency increases, thus resulting in a higher crystallization temperature as seen in Figure 4b.

4. Temperature Dependence of Gas Permeation Properties. For a temperature range that does not involve thermal transition, there is a logarithmic relationship between permeability P and $1/T$ which could be described by a van't Hoff−Arrhenius equation.

$$P = P_0 \exp(-E_p/RT) \quad (7)$$

where P_0 is the pre-exponential factor, E_p is the apparent activation energy for permeation, R is gas constant, and T is the absolute temperature. The temperature dependence of diffusivity and solubility can also be described by similar equations as follows:

$$D = D_0 \exp(-E_d/RT) \quad (8)$$

$$S = S_0 \exp(-H_s/RT) \quad (9)$$

where S_0 and D_0 are the pre-exponential factors, H_s is the activation energy for diffusion, and E_d is the heat of sorption. Only several researchers had done their research in the temperature range that involves the thermal transition. Mogri and Paul[31,32] developed a system to monitor the permeability change before and after side chain melting in acrylates. They found that both diffusivity and solubility increased above the melting temperature due to lower diffusion activation energy in the molten state and an increase in sorption sites. Okamoto et al.,[33] Hirayama et al.,[34] and Kim et al.[35] have individually observed discontinuity in the ln P vs $1/T$ curve in their PEO-based polymer systems. Abrupt points around the melting temperatures indicate that the permeability jumps could be attributed to the melting of PEO crystals. However, detailed analyses on the temperature dependence of the selectivity, especially for the CO_2/H_2 selectivity, have not been addressed.

Figure 5 shows the temperature dependence of permeability measured at 30−50 °C and 2 atm. A similar permeability discontinuity is observed, especially for those with a higher PEG-azide loading. Below the melting temperature, PEG-azide crystals are impermeable physical obstacles that impede gas transport. In addition, the existence of crystalline domains restricts the chain motion in amorphous regions. Thus, the permeability declines with increased crystallinity. GPA1100-40 shows the lower permeability below the melting temperature, while GPA1100-20 possesses the higher one. After the crystals melt, the permeability increases with increasing EO group concentration. Therefore, the permeability trend above melting temperature is reversed. For GPA1100-40, the CO_2 permeability could reach as high as 1052 barrer at 2 atm and 50 °C. Permeability jumps happen between 35 and 40 °C; however, the melting points measured by DSC are larger than 40 °C as shown in Table 1. This may be caused by the temperature lag in the dynamic DSC measurement as well as the facilitated melting at the presence of compressed CO_2 (discussed later).[36]

Figure 6a,b presents the temperature dependence of CO_2 sorption isotherms of GPA1100-20 and GPA1100-40. Most of the isotherm curves are linear except for GPA1100-40 at 35 °C, where the sorption isotherm curves show a nonlinear progression when the pressure increases. The nolinear sorption isotherm could be explained by the CO_2-induced plasticization.[29,36] The dissolved CO_2 in the polymer matrix disassociate polymer chains, thus lowering the melting temperature of PEG-azide. Simultaneously, more effective EO groups are released because of the melting, which further increases the sorption of CO_2. When the loading of PEG-azide is low, this phenomenon is not obvious. However, when the PEG-azide content increases, plasticization caused sorption increases so that the GPA1000-40 isotherm shows an upward trend at 35 °C. The solubility coefficient for the linear sorption isotherm is obtained by fitting the slope, while dC/dp at 2 atm is used to calculate the solubility

Table 4. Pure Gas Permeability and Selectivity of GPA1100 Series before and after Grafting

sample	temp (°C)	H_2 permeability (barrer)[a]	N_2 permeability (barrer)	CO_2 permeability (barrer)	CO_2/H_2 selectivity	CO_2/N_2 selectivity
GPA1100-20	35	36.7	7.54	321	8.7	43
	45	62.3	13.9	468	7.5	34
GPA1100-20 after grafting	35	70.4	13.6	595	8.5	44
	45	106	19.4	695	6.6	36
GPA1100-40	35	22.0	4.62	247	11.2	53
	45	91.0	22.6	982	10.8	43
GPA1100-40 after grafting	35	61.1	10.5	513	8.4	49
	45	222	50.5	1840	8.3	36

[a] 1 barrer = 10^{-10} cm^3 (STP) cm/(cm^2 s cmHg).

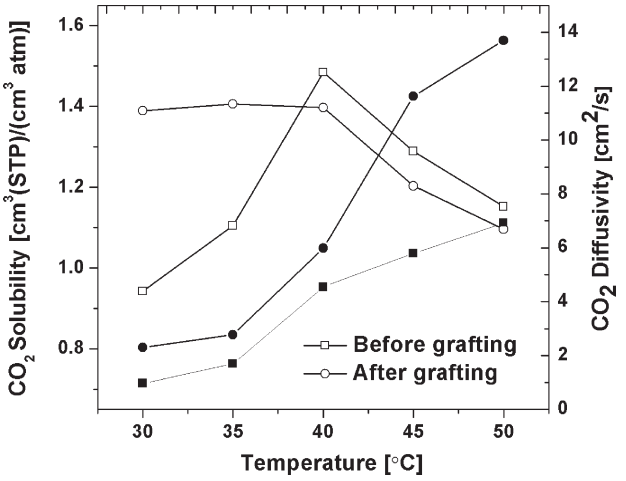

Figure 12. CO_2 solubility (open) and diffusivity (solid) of GPA1100-40 before and after grafting.

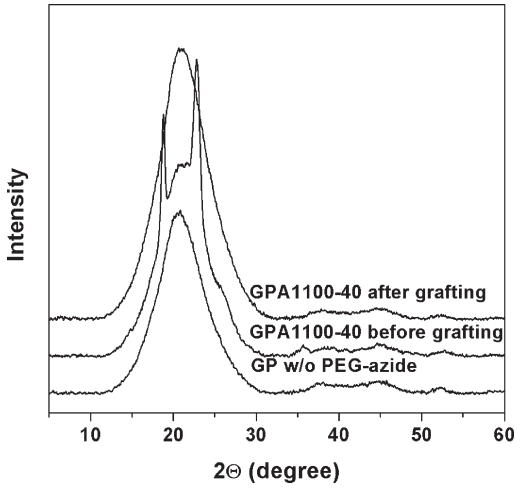

Figure 13. Wide-angle XRD patterns of GP w/o PEG-azide and GPA1100-40 before and after the grafting at ambient temperature.

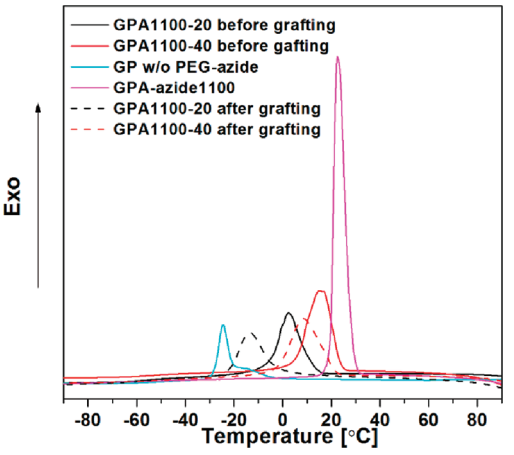

Figure 14. Second cooling curve of GPA1100-20 and GPA1100-40 before and after the grafting.

for the nonlinear isotherms. Figure 7a shows the temperature dependence of CO_2 solubility and N_2 solubility. The peak-shaped curves of solubility are observed for CO_2, while N_2 solubility always increases with increasing temperature.[34] Below the melting temperature, the solubility is proportional to the volume fraction of amorphous regions; the solubility therefore decreases with more PEO-azide loading (i.e., higher overall crystallinity). After the crystals melt, this trend is reversed because OIMs with more liquid PEO-azide have more EO groups favorable for CO_2 sorption. When the temperature further increases, CO_2 solubility decreases because the heat of sorption (H_s) is negative in PEO based membranes.[34,35] N_2 solubility of these OIMs always increases despite the thermal transition because H_s is always positive for N_2.[34,35] H_2 sorption in this kind of material is too low to be measured accurately. However, we believe that the H_2 solubility would not change too much when the temperature varies. Figure 7b shows the temperature dependence of CO_2 diffusivity in GPA1100-20 and GPA1100-40. The diffusivity below the melting points is comparable. Nevertheless, the diffusivity of GPA1100-40 increases tremendously after PEG-azide melts because of the high PEG-azide content. The temperature dependence of the solubility and diffusivity could be further related to the CO_2/H_2 and CO_2/N_2 permselectivity, as shown in Figure 8a,b. GPA1100-20 shows the highest CO_2/H_2 permselectivity at 40 °C, which is the same temperature that the highest CO_2 solubility is obtained. It is believed that the highest permeability selectivity comes from the highest solubility selectivity because the selectivity in rubbery materials is governed by the solubility selectivity. With more EO groups, the solubility selectivity increases, thus resulting in a high selectivity of GPA1100-40 (12.3) than that of GPA1100-20 (8.5). CO_2/N_2 permselectivity always declines with rising temperature due to the decreasing

CO_2/N_2 solubility selectivity and the weakened size sieving effect.

5. Thermal Grafting of PEG-azide and Characterizations. Azido groups are linear 1, 3-dipolar structures that could easily form nitrenes, which are highly reactive and short-lived nitrogen intermediates, with the presence of ultraviolet radiation or heat. Nitrenes have four nonbonded electrons so that they could insert into C−H bonds, following the reactivity order of tertiary > secondary > primary C−H bonds.[37,38] The most possible thermal grafting mechanism is shown in Figure 1. The activated nitrenes attack the tertiary C−H bonds of PPO segments and form C−N bonds at 140 °C under vacuum. ^{13}C solid-state NMR spectra in Figure 9 show the chemical environment change after thermal grafting. By comparing Figure 9a (GPA1100-40 pristine) and Figure 9b (GPA1100-40 after thermal grafting), small peaks belonging to $-CH_2-N_3$ (g; δ = 51 ppm)[39] disappear, indicating that azide groups are fully reacted. This correlates well with the nitrogen 1s binding energies change characterized by XPS, as shown in Figure 10. Before thermal grafting, two distinct peaks (405 and 401 eV) with a peak areas ratio of 1:2 are assigned to the central, electron-deficient nitrogen and the other two nitrogen atoms in the azide group, respectively.[40] A small shoulder peak at 399 eV corresponding to the organic C−N bond[40] is also observed due to the existence of amine groups during matrix synthesis. Reaction of nitrenes with C−H bonds via insertion reduces the 401 and 405 eV peak to the level of noise. However, the intensity or the peak area of C−N bond increases after thermal grafting, thus indicating the successful conversion of $C-N_3$ groups into C−NH groups. Peak c (δ = 70.3 ppm) in Figure 9a,b is normally assigned to the CH_2 of PEG, while peaks d (δ = 74.8 ppm) and e (δ = 71.7 ppm) are assigned to CH_2 and CH of poly(propylene glycol).[41] Peak a (δ = 9.07 ppm), peak f (δ = 17.0 ppm), and peak b (δ = 22.9 ppm) at a lower δ value are assigned to the carbons of the aliphatic part, as shown in Figure 9a,b. After PEG-azide grafting, the relative intensity of the CH moiety (peak e) decreases, and a small shoulder peak at a higher δ value is observed. Part of e-type carbons are connected to the nitrogen atoms which are more electronegative than the hydrogen atoms. Thus, chemical shift of the carbon atoms at the grafting point moves to a higher δ value. Other types of grafting have not been seen in ^{13}C NMR spectra, which might be caused by their relative low reactivity and the low sensitivity of solid-state ^{13}C NMR. At 140 °C, only grafting reactions are activated. The self-decomposition of PEG-azide1000 starts at 240 °C as seen from TGA in Figure 11.

6. Gas Permeation Properties after Thermal Grafting. Gas permeability is almost doubled, and the selectivity only slightly decreases after thermal grafting as depicted in Table 4. The highest CO_2 permeability obtained is 1840 barrer with CO_2/H_2 and CO_2/N_2 selectivity of 8.3 and 36 at 2 atm and 45 °C. Compared to the pristine substrate (GP w/o PEG-azide), the permeability is almost improved by 5-fold and the selectivity even slightly increases. With PEG grafting on the backbone of OIMs, the crystallization tendency is greatly depressed because PEG-azide is partially immobilized. The polymer chains of the blended PEG cannot be rearranged easily and will create lots of chain ends and voids within the "mesh" of the OIMs. Therefore, the diffusivity will increase due to more free volume created by these irregular chain ends and voids. Figure 12 shows the CO_2 diffusivity and solubility changes after thermal grafting of GPA1100-40. The CO_2 diffusivity shows a great improvement at any temperature. However, the CO_2 solubility shows enhancement only below the melting temperature in pristine GPA1100-40. Above the melting point, the solubility is slightly lower than that before grafting. This could be ascribed to the partial immobilization of PEG-azide. Fewer EO groups are involved in the CO_2 sorption because some of the EO groups are not available due to the steric hindrance. The increment of solubility at 30 and 35 °C could be attributed to the amorphous nature of GPA1100-40 after grafting. Figure 13 shows the WXRD patterns at ambient temperature of GP w/o PEG-azide and GPA1100-40 before and after grafting. GP w/o PEG-azide is amorphous because of the cross-linked structure. GPA1100-40 is a semicrystalline membrane at room temperature, which has two characteristic crystal peaks of PEO located at 2θ = 19.2 and 23.3.[42] With the PEG grafting, GPA1100-40 does not shows obvious crystal peaks. DSC cooling curves have also revealed the suppressed crystallization tendency after grafting as shown in Figure 14. The crystallization temperatures of GPA1100-20 and GPA1100-40 drop from 2.5 and 16.1 °C to −13.4 and 8.5 °C after grafting, respectively. Exclusion from crystallization at ambient temperature makes these OIMs more valuable for CO_2 separation in a broad temperature range. These preliminary results have shown a promising method to further improve CO_2 permeability of the OIMs.

CONCLUSIONS

We have demonstrated strategies to increase CO_2 permeability without sacrificing the selectivity for the CO_2 selective OIMs. PEG terminated with one azide and one methoxy group tends to enhance the CO_2 permeability by 2-fold compared to that with hydroxyl end groups. A permeability jump is observed when the temperature surpasses the melting point of PEG-azide. The temperature dependences of permeability, solubility, diffusivity, and selectivity are discussed in detail. Maxima of CO_2 solubility and CO_2/H_2 permselectivity are obtained in a given temperature range. An attempt to graft PEG chains onto the backbone of the OIMs via azide reaction has been made. Solid-state ^{13}C NMR, XPS, and TGA indicate that the PEG-azide has been successfully grafted. CO_2 permeability increases by 5-fold for grafted membranes as compared with the ungrafted substrate. The crystallization tendency of the grafted membrane has been greatly depressed. Diffusivity increment is believed to be the major reason for the permeability enhancement. Extremely high CO_2 permeability makes these OIMs great potential as commercial membrane materials for CO_2 capture. However, it is still a long way to fabricate these materials into hollow fibers or asymmetric membranes with a separation layer thickness in the range of 100 nm. Work on making these materials into multilayer thin film composite membranes by continuous coating[43,44] is ongoing in our group. Because PEO based materials are hydrophilic and mechanically weak compared to the conventional glassy polymers, future studies focused on the long-term stability under water vapor exposure and various gas mixtures feed are critical to the next step of development.

ACKNOWLEDGMENT

The authors thank NUS graduate school of integrative science and engineering for Mr. Xia's scholarship and the Singapore National Research Foundation (NRF) for the support on the project entitled "Molecular Engineering of Membrane Materials: Research and Technology for Energy Development of Hydrogen, Natural Gas and Syngas" with grant R-279-000-261-281.

The authors also want to express their gratitude to Prof. D. R. Paul (University of Texas, Austin), Prof. Lu Shao (Harbin Institute of Technology, China), Dr. Youchang Xiao, Mr. Cher Hon Lau, and other colleges in our group for their valuable discussions and help.

REFERENCES

(1) Spahni, R.; Chappellaz, J.; Stocker, T. F.; Loulergue, L.; Hausammann, G.; Kawamura, K.; Flückiger, J.; Schwander, J.; Raynaud, D.; Masson Delmotte, V.; Jouzel, J. *Science* **2005**, *310*, 1317–1321.
(2) Siegenthaler, U.; Stocker, T. F.; Monnin, E.; Lüthi, D.; Schwander, J.; Stauffer, B.; Raynaud, D.; Barnola, J. M.; Fischer, H.; Masson Delmotte, V.; Jouzel, J. *Science* **2005**, *310*, 1313–1317.
(3) Hoffert, M. I.; Caldeira, K.; Benford, G.; Criswell, D. R.; Green, C.; Herzog, H.; Jain, A. K.; Kheshgi, H. S.; Lackner, K. S.; Lewis, J. S.; Lightfoot, H. D.; Manheimer, W.; Mankins, J. C.; Mauel, M. E.; Perkins, L. J.; Schlesinger, M. E.; Volk, T.; Wigley, T. M. L. *Science* **2002**, *298*, 981–987.
(4) Rochelle, G. T. *Science* **2009**, *325*, 1652–1654.
(5) Schrag, D. P. *Science* **2007**, *315*, 812–813.
(6) Haszeldine, R. S. *Science* **2009**, *325*, 1647–1652.
(7) Merkel, T. C.; Lin, H.; Wei, X.; Baker, R. *J. Membr. Sci.* **2010**, *359*, 126–139.
(8) Koros, W. J.; Madden, W. C. *Transport Properties*; John Wiley & Sons, Inc.: New York, 2002.
(9) Wind, J. D.; Sirard, S. M.; Paul, D. R.; Green, P. F.; Johnston, K. P.; Koros, W. J. *Macromolecules* **2003**, *36*, 6433–6441.
(10) Achalpurkar, M. P.; Kharul, U. K.; Lohokare, H. R.; Karadkar, P. B. *Sep. Purif. Technol.* **2007**, *57*, 304–313.
(11) Merkel, T. C.; Bondar, V. I.; Nagai, K.; Freeman, B. D.; Pinnau, I. *J. Polym. Sci., Part B: Polym. Phys.* **2000**, *38*, 415–434.
(12) Lin, H.; Freeman, B. D. *J. Membr. Sci.* **2004**, *239*, 105–117.
(13) Lin, H.; Freeman, B. D. *J. Mol. Struct.* **2005**, *739*, 57–74.
(14) Chen, H.; Xiao, Y.; Chung, T. S. *Polymer* **2010**, *51*, 4077–4086.
(15) Husken, D.; Feijen, J.; Gaymans, R. J. *J. Polym. Sci., Part A: Polym. Chem.* **2007**, *45*, 4522–4535.
(16) Lin, H.; Van Wagner, E.; Freeman, B. D.; Toy, L. G.; Gupta, R. P. *Science* **2006**, *311*, 639–642.
(17) Kawakami, M.; Iwanaga, H.; Hara, Y.; Iwamoto, M.; Kagawa, S. *J. Appl. Polym. Sci.* **1982**, *27*, 2387–2393.
(18) Car, A.; Stropnik, C.; Yave, W.; Peinemann, K. V. *J. Membr. Sci.* **2008**, *307*, 88–95.
(19) Car, A.; Stropnik, C.; Yave, W.; Peinemann, K. V. *Adv. Funct. Mater.* **2008**, *18*, 2815–2823.
(20) Car, A.; Stropnik, C.; Yave, W.; Peinemann, K. V. *Sep. Purif. Technol.* **2008**, *62*, 110–117.
(21) Yave, W.; Car, A.; Funari, S. S.; Nunes, S. P.; Peinemann, K. V. *Macromolecules* **2010**, *43*, 326–333.
(22) Yave, W.; Car, A.; Peinemann, K. V. *J. Membr. Sci.* **2010**, *350*, 124–129.
(23) Yave, W.; Car, A.; Peinemann, K. V.; Shaikh, M. Q.; Rätzke, K.; Faupel, F. *J. Membr. Sci.* **2009**, *339*, 177–183.
(24) Shao, L.; Chung, T. S. *Int. J. Hydrogen Energy* **2009**, *34*, 6492–6504.
(25) Xia, J.; Liu, S.; Lau, C. H.; Chung, T. S. *Macromolecules* **2011**, *44*, 5268–5280.
(26) Lau, C. H.; Liu, S.; Paul, D. R.; Xia, J.; Jean, Y. C.; Chen, H.; Shao, L.; Chung, T. S. *Adv. Energy Mater.* **2011**, *1*, 634–642.
(27) Lin, W. H.; Vora, R. H.; Chung, T. S. *J. Polym. Sci., Polym. Phys.* **2000**, *38*, 2703–2713.
(28) Chung, T. S.; Chan, S. S.; Wang, R.; Lu, Z.; He, C. *J. Membr. Sci.* **2003**, *211*, 91–99.
(29) Reijerkerk, S. R.; Nijmeijer, K.; Ribeiro, C. P., Jr.; Freeman, B. D.; Wessling, M. *J. Membr. Sci.* **2011**, *367*, 33–44.
(30) Nandan, B.; Hsu, J. Y.; Chen, H. L. *Polym. Rev.* **2006**, *46*, 143–172.
(31) Mogri, Z.; Paul, D. R. *J. Membr. Sci.* **2000**, *175*, 253–265.
(32) Mogri, Z.; Paul, D. R. *Polymer* **2001**, *42*, 2531–2542.
(33) Okamoto, K. i.; Fuji, M.; Okamyo, S.; Suzuki, H.; Tanaka, K.; Kita, H. *Macromolecules* **1995**, *28*, 6950–6956.
(34) Hirayama, Y.; Kase, Y.; Tanihara, N.; Sumiyama, Y.; Kusuki, Y.; Haraya, K. *J. Membr. Sci.* **1999**, *160*, 87–99.
(35) Kim, J. H.; Ha, S. Y.; Lee, Y. M. *J. Membr. Sci.* **2001**, *190*, 179–193.
(36) Wang, J. S.; Kamiya, Y.; Naito, Y. *J. Polym. Sci., Part B: Polym. Phys.* **1998**, *36*, 1695–1702.
(37) Low, B. T.; Chung, T. S.; Chen, H.; Jean, Y. C.; Pramoda, K. P. *Macromolecules* **2009**, *42*, 7042–7054.
(38) Moody, C. J.; Whitham, G. B. *Reactive Intermediates*; Oxford University Press: New York, 1992.
(39) Lammens, M.; Skey, J.; Wallyn, S.; O'Reilly, R.; Du Prez, F. *Chem. Commun.* **2010**, *46*, 8719–8721.
(40) Collman, J. P.; Devaraj, N. K.; Eberspacher, T. P. A.; Chidsey, C. E. D. *Langmuir* **2006**, *22*, 2457–2464.
(41) Brandolini, A. J.; Hills, D. D. *NMR Spectra of Polymers and Polymer Additives*; Marcel Dekker: New York, 2000.
(42) Wang, H.; Keum, J. K.; Hiltner, A.; Baer, E. *Macromol. Rapid Commun.* **2010**, *31*, 356–361.
(43) Chung, T. S.; Kafchinski, E. R.; Kohn, R. S.; Foley, P.; Straff, R. S. *J. Appl. Polym. Sci.* **1994**, *53*, 701–708.
(44) Shieh, J. J.; Chung, T. S.; Paul, D. R. *Chem. Eng. Sci.* **1999**, *54*, 675–684.